



HAL
open science

Numerical simulation of the force generated by a superelastic NiTi orthodontic archwire during tooth alignment phase: comparison between different constitutive models

M Gannoun, M Laroussi Hellara, Céline Bouby, Tarak Ben Zineb, T Bouraoui

► To cite this version:

M Gannoun, M Laroussi Hellara, Céline Bouby, Tarak Ben Zineb, T Bouraoui. Numerical simulation of the force generated by a superelastic NiTi orthodontic archwire during tooth alignment phase: comparison between different constitutive models. *Materials Research Express*, 2018, 5 (4), pp.045405. 10.1088/2053-1591/aaba4d . hal-01771358

HAL Id: hal-01771358

<https://hal.science/hal-01771358>

Submitted on 7 Jan 2020

HAL is a multi-disciplinary open access archive for the deposit and dissemination of scientific research documents, whether they are published or not. The documents may come from teaching and research institutions in France or abroad, or from public or private research centers.

L'archive ouverte pluridisciplinaire **HAL**, est destinée au dépôt et à la diffusion de documents scientifiques de niveau recherche, publiés ou non, émanant des établissements d'enseignement et de recherche français ou étrangers, des laboratoires publics ou privés.



Distributed under a Creative Commons Attribution 4.0 International License

Numerical simulation of the force generated by a superelastic NiTi orthodontic archwire during tooth alignment phase: Comparison between different constitutive models

M. Gannoun^a, M. Laroussi Hellara^a, C. Bouby^b, T. Ben Zineb^b and T. Bouraoui^{a, *a} ENIM, LGM, University of Monastir, Tunisia

^b LEM3, University of Lorraine, CNRS, UMR 7239, Vandoeuvre les-Nancy, France

*Tarak.bouraoui@gmail.com

Abstract:

Nickel Titanium (NiTi) Superelastic (SE) Shape Memory Alloys (SMAs) are widely considered for applications that need high reversible strain or high recovery forces. In particular, the SE SMAs present a high interest for biomedical applications such as endodontic and orthodontic apparatus. They are available in a large variety of archwires exerting continuum forces to ensure the dental displacement.

The purpose of this study is to report the clinical implications of NiTi SE wires for dental treatment in a given configuration.

Three main constitutive models of the literature (Lagoudas and Boyd 1996, Auricchio and Petrini 2004 and Chemisky et al 2011) are considered for the finite element (FE) numerical simulations of the SMA archwires response. Tensile tests had been carried out in order to identify the material parameters of these constitutive models. The FE numerical study allowed to predict the dental displacement and its corresponding orthodontic force level exerted by the wire in similar conditions to those in the oral environment.

This work allows to predict the orthodontic generated load by a NiTi SE archwire with a $0.64 \times 0.46 \text{ mm}^2$ rectangular cross section under prescribed thermomechanical conditions. The effect of the temperature and the alveolar bone stiffness on the orthodontic load level and the tooth displacement degree has been investigated.

The performed numerical simulations demonstrate that the orthodontic load is sensitive to the displacement magnitude, to the tooth stiffness and to the temperature variations. The obtained forces applied continuously and at a constant level are within the acceptable orthodontic force level range. Some directives are therefore provided to help orthodontists to select the optimal archwire.

Keywords: NiTi, Superelasticity, Orthodontic archwire, Finite elements, Numerical simulation, Phenomenological models.

1. Introduction

The orthodontic archwires are used to align and correct a mis-positioned tooth. The archwire applies a load that causes the dental displacement. The choice of an archwire depends conventionally on its capacity to induce an adapted and continuum loading after fixation, making possible for the tooth position to be corrected.

NiTi Shape Memory Alloys (SMAs) have been highly considered in the orthodontic field since their introduction by Andersean (1971). In fact, they have very interesting properties such as an excellent corrosion resistance, a high biocompatibility with human natural system, a low elasticity modulus and an important elastic force delivery range (Their et al 2004).

Within the last decade, many new NiTi orthodontic wires have been introduced. Some of them possess the superelasticity property. This property enables the SMA to recover large inelastic strains (about 10 %) due to a reversible thermoelastic martensitic transformation (Andersean et al 1971).

The introduction of NiTi archwires has revolutionized the orthodontic field. They generate during the unloading step low constant forces over a wider range of displacements than the traditional wires (Aghili et al 2017, Miura et al 1986).

Therefore, the main challenge is to overcome the difficulty to determine the optimal orthodontic arches due to the large number of the involved factors in the oral cavity (Tanne et al 1987). Moreover, the information on the forces exerted by the archwire on the tooth in a dental brace is of a high importance for the orthodontists and patients. In this way, it will be possible for clinicians to adjust the wires placed in the mouth in order to guarantee an adequate exerted force allowing to align the teeth quickly and painlessly for the patient. Indeed, efficient tooth movement depends on several physiological and mechanical conditions correlated with the alveolar bone response (Schneider et al 2002). A numerical study thereby seems to be a powerful tool in order to identify the optimal orthodontic force for a particular clinic situation. Hence, the main challenge is the finite element numerical simulation of the complex response of the system NiTi archwire and teeth in order to accurately predict the needed force for the teeth position correction (Segner and Ibe 1995).

Actually, there is a limited number of studies that numerically investigated orthodontic loads in literature (Rudolf et al 2013). Most of the studies predicting the orthodontic force at several applied deflections focused on the comparison of different commercial wires (Bourauel et al 1999, Lombardo et al 2012). Aghili et al (2015) performed the load-deflection of three wire designs and concluded that the type of archwire and brackets significantly affected the load level.

This work aimed to present a comparison between models to accurately predict the load level for different displacements during the dental treatment. The main objective is to investigate the ability of each model to predict the magnitude of the generated force by orthodontic wires under different prescribed conditions, temperatures and alveolar bone stiffness.

This investigation attempts to approximate clinical conditions in a deflection test of loading and unloading upon a given dental configuration. In the first part is presented a characterization of the SMA allowing to identify the material parameters of the three considered constitutive models. These three constitutive models are then adopted to simulate the orthodontic load. Finally, the influence of the temperature and the bone stiffness on the load level has been investigated.

2. Material characterization and constitutive models

2.1. Material

The studied archwire is processed with a $\text{Ti}_{50.8}\text{-Ni}_{48.2}$ SMA and has a $0.64 \times 0.46 \text{ mm}^2$ rectangular cross section as in Gamaoun et al (2011) study. This commercial SMA is marketed in a pre-formed archwire shape for orthodontic applications.

2.2. Experimental characterization

In order to investigate the superelastic behavior and to identify the mechanical properties of the SMA, tensile tests have been carried out, at constant temperature of 35°C on lengths of 40 mm of the archwire specimens were tested under uniaxial tension. The mechanical behavior has been characterized under a tensile machine LLOYD INSTRUMENTSTM, LR5KPlus Series with a maximum loading cell of 20 kN. The specimen has been charged at a strain rate of $6.66 \cdot 10^{-3} \text{ s}^{-1}$ to a maximum strain of 7%. The obtained results have been post-treated with the software “NEXYGEN”.

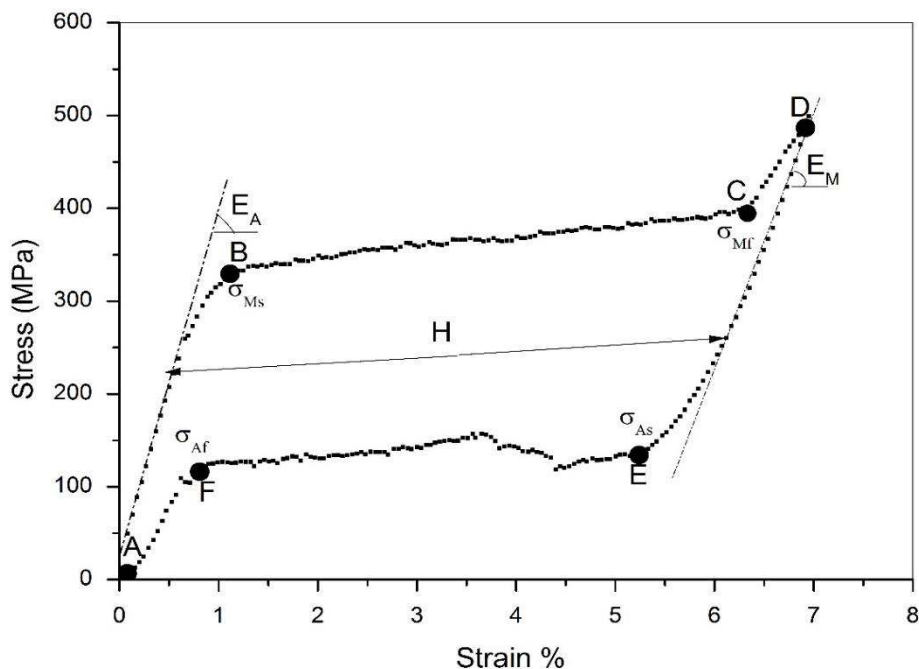


Figure 1. Tensile behavior of $\text{Ni}_{50.8}\text{Ti}_{48.2}$ at 35°C loaded with a $6.66 \cdot 10^{-3} \text{ s}^{-1}$ strain rate to 7 % of strain.

The NiTi SMA exhibits a superelastic behavior at the oral temperature 35°C as shown in Figure 1. This figure shows that the stress-strain curve exhibits four different behaviors. Loading starting from

point A leads to an elastic response of the SMA initially in the austenitic state with an elastic modulus E_A up to B where the transformation to martensite occurs at a yield stress σ_{Ms} . Then a pseudo-plateau BC is observed corresponding to an increase in strain with a quasi-constant stress. At point C the material is fully martensitic at a σ_{Mf} stress. The slope CD represents the elastic response of martensite. At point D the material is still fully martensitic. During the unloading, the slope DE corresponds to the elasticity of the martensite with an elastic modulus E_M . The reverse transformation occurs slightly before point E , corresponding to a yield stress σ_{As} . Between E and F , the reverse transformation is activated, with a hysteresis H , induced by unloading. Finally, an elastic unloading between F and A occurs at a σ_{Af} stress level. The corresponding set of material parameters is identified within this tensile test is presented in Table 1.

Table 1. Experimental material parameters

σ_{Ms} (MPa)	σ_{Mf} (MPa)	σ_{As} (MPa)	σ_{Af} (MPa)	H (%)	E_A (MPa)	E_M (MPa)
335	390	120	105	5.18	36000	25000

During the orthodontic treatment, the tooth movement is acted by the applied loading delivered by the orthodontic wire during the unloading. Hence, the SMA is loaded at $\sigma < \sigma_{Ms}$ without the activation of the martensitic transformation. If the loading is at a stress state σ between σ_{Ms} and σ_{Mf} , the unloading curve goes down then the stress level decreases till σ_{Af} . In fact, the inner loops appear when the forward transformation ceases before reaching the complete fully martensitic phase (loading to 7% in figure 2). The formulation of the inner loops was considered based on the major hysteresis cycle. Many developed models were able to describe the inner loops feature (Muller 1989, Gillet et al 1998, Peultier et al 2006, Bouvet et al 2004). This means that the unloading curve does not necessary intersect the diagonal of the complete hysteresis, this depends on the considered formulation. In the case of orthodontic wire application, the knowledge of only partial loops may be significant to determinate a response. Those wires could be also subjected to loading and unloading cycles at different loading amplitudes to deliver constant forces over tooth aligning and movement (Miura et al 1986).

Figure 2 illustrates the inner loop feature at different strain unloading levels and is comparable to many experimental tests such as Dolce and Cordane (2001). In clinics, the interest of this property is to quantify the real corresponding load for different tooth displacement of the loaded SMA wire could be achieved in the plateau without reaching the end of the martensitic transformation. The unloading curve seems following the elastic part of the reverse transformation until reaching the diagonal of complete cycle and keeps coming down linearly. The unloading pseudo-plateau takes place at a higher stress value than the complete reverse transformation yield stress. In consequence, it is important to

evaluate as accurately as possible the orthodontic applied loading by taking into account the effect of the inner loops.

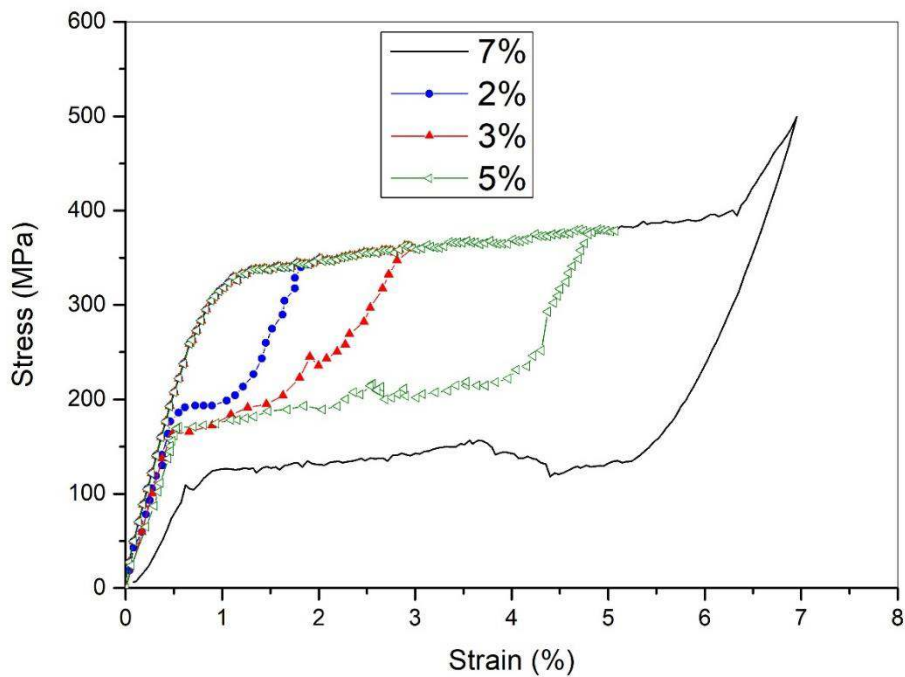


Figure 2. Experimental inner loops behavior of a NiTi virgin wire at 2%, 3%, 5% and 7% of strains with $\dot{\epsilon} = 6.66 \cdot 10^{-3} s^{-1}$.

In addition to tensile test, a Differential Scanning Calorimetric (DSC) test was carried out in order to identify the forward and reverse start and finish temperatures (M_s , M_f , A_s and A_f). This measure was obtained during a heating-cooling cycle between $-100^{\circ}C$ and $100^{\circ}C$. The DSC test results are shown in Figure 3. The transformation temperatures are identified by plotting the tangents to different peaks (see Figure 3). It is worth noting that the SE SMA is at the austenitic state at the oral ($35^{\circ}C$) and room ($25^{\circ}C$) temperatures. We note that the heating curve presents the R-phase transformation.

The abbreviations labeled on the graph indicate the martensite start and finish transformation temperatures respectively M_s and M_f characterizing the forward transformation. A_s and A_f indicate austenite start and finish temperatures characterizing the reverse transformation.

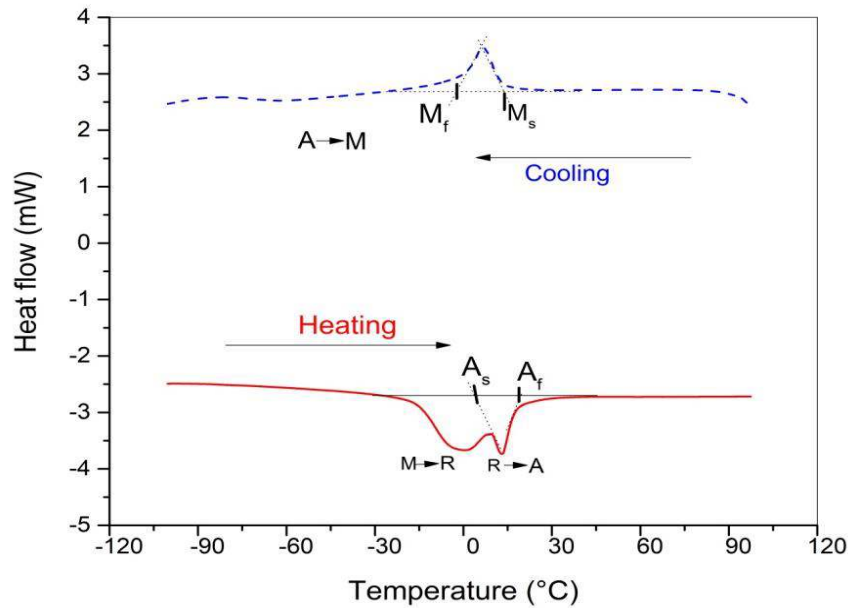


Figure 3. NiTi as-received archwire DSC curves.

2.3. Constitutive models

In the literature there are many proposed approaches to define the thermomechanical constitutive laws for shape memory alloys. Usually, these approaches can predict the superelastic and the shape memory effect behaviors. They are also able to describe other effects such as the detwinning of the martensite, the asymmetric responses in tension and compression and the inner cycles (Cisse et al 2016). Some researchers classified models into (i) micro-macro models that describe the behavior of each single grain and derive the polycrystalline macroscopic effective behavior using a scale transition technique as self-consistent or Mori-Tanaka techniques, and (ii) phenomenological models that directly represent the material behavior at the macroscopic scale, starting from the evolution of internal variables defined at the macro-scale (Cisse et al 2016).

In order to predict, by finite element, the induced force during the inner loop behavior, three models developed within the framework of phenomenological thermomechanics with internal variables were considered. The first behavior model was proposed by Lagoudas and Boyd (1996) and it is available in an open source. The second behavior model was developed by Auricchio and Petrini (2004). It is an improved version the model of Souza et al (1998) and it is already available in the finite element code Abaqus. The third model was developed by Chemisky et al (2011) and implemented in Abaqus via the UMAT subroutine.

The Lagoudas and Boyd (1996) and Chemisky et al (2011) models are based on the expression of Gibbs free energy whereas the model of Auricchio and Petrini (2004) is derived from Helmholtz free energy expression. Table 2 presents a brief sum up of the different properties reproduced by the three models involved in this study.

Table 2. Summary of aspects reproduced by considered models.

	Lagoudas and Boyd 1996	Auricchio and Petrini 2004	Chemisky et al 2011
Elastic modulus of A and M	$E_A \neq E_M$	$E_A \neq E_M$	$E_A = E_M$
Twinned martensite	Yes	Yes	Yes
Detwinned martensite	No	No	Yes
Asymmetry tension- compression	No	Yes	Yes
Inner loops	No	Yes	Yes
Cycling	No	No	No
Variables of control	T, σ	T, ε	T, σ
Internal variables	$\underline{\varepsilon}^{tr}, g^t, \xi$	$\underline{\varepsilon}^{tr}$	$\xi, \underline{\varepsilon}^{tr}, \underline{\varepsilon}^{twin}$
Large deformation	No	No	No
Anisotropic behavior	No	No	No

ε^{tr} is the martensitic transformation strain, ξ is the volume fraction of martensite, the ε^{twin} is the mean strain induced twinning martensite and g^t is the transformation hardening-like energy.

To test the model's capabilities to predict the main features of NiTi SMAs which are the superelasticity (SE) and the inner loops, several uniaxial stress-strain have been processed under stress control will be described.

For that end, finite element model with a three-dimensional unit cube (1 mm × 1 mm × 1 mm) subjected to uniaxial loading-unloading cycle in tension at a constant temperature-is considered. The cube consists in a single eight-node brick finite element (labeled C3D8 in Abaqus finite element code). The material parameters of each model are identified from experimental uniaxial stress strain curves (Figure 1).

The cube is constrained with symmetry conditions correlated with a uniaxial loading test. The numerical test is made in two steps:

- Step 1: application of a displacement (strain) of 0.07 mm along z direction in the nodes corresponding to the free face of the cube;
- Step 2: release of the displacement condition to recover the strain;

Table 3, Table 4 and Table 5 show the corresponding set of material parameters used for each adopted model which have been identified within the experimental tests.

Table 3. Lagoudas UMAT material properties.

E_A	36000 MPa
E_M	25000 MPa
$\nu_A = \nu_M$	0.33
$\alpha_A = \alpha_M$	22.10^{-6}K^{-1}
$\varepsilon_{\max}^{\text{tr}} = H$	5.2 %
M_s	5 °C
M_f	-1 °C
A_s	3 °C
A_f	17 °C
$\rho\Delta s_A$	-0.44 MPa.C ⁻¹
$\rho\Delta s_M$	-0.17 MPa.C ⁻¹

Accordingly, ν is the Poisson ratio, α is the thermal expansion coefficient, H or $\varepsilon_{\max}^{\text{tr}}$ is the maximum transformation strain. $\rho\Delta s_i$ ($i=A$ or M) are the coefficient of stress influence or the slopes of direct and reverse martensitic transformation in the (σ, T) curve (Lagoudas and Boyd 1996) :

$$\rho\Delta s^M = - \frac{\sigma A_s}{T_{\text{test}} - M_s} H ; \rho\Delta s^A = - \frac{\sigma M_s}{T_{\text{test}} - A_s} H$$

where T_{test} is the temperature of the superelastic test.

Table 4. Chemisky UMAT material properties.

$E_A = E_M$	36000 MPa
ν	0.33
$\alpha_A = \alpha_M$	22.10^{-6}C^{-1}
$\varepsilon_{\max}^{\text{tr}} = H$	5.2 %
$\varepsilon_{\text{tracmax}}^{\text{TFA}}$	0.04
$\varepsilon_{\text{compmax}}^{\text{TFA}}$	0.04
b_d	4.2 MPa.C ⁻¹
b_r	1.7 MPa.C ⁻¹
A_f	17 °C
M_s	5 °C
r_f	0.6
F_ε	100 MPa
H_f	4 MPa

where $\varepsilon_{\text{tracmax}}^{\text{TFA}}$ and $\varepsilon_{\text{compmax}}^{\text{TFA}}$ are respectively the maximum transformation strain and the maximum strain of auto-accommodate martensite.

b_d and b_r are defined to describe respectively the slopes of direct and reverse martensitic transformations in the (σ, T) curve. r_f is the internal loops amplitude coefficient, F_ε is the yield stress of the reorientation process start and H_f denotes the pseudo-hardening coefficient of the martensitic transformation. r_f , F_ε and H_f are taken from experiments done by Lachiguer et al (2016).

Table 5. Auricchio UMAT material properties.

E_A	33000 MPa
E_M	25000 MPa
ν	0.33
$\varepsilon_{\max}^{\text{tr}}$	5.2 %
$\rho\Delta s_A$	0.44 MPa.C ⁻¹
σ_L^S	335 MPa
σ_L^E	390 MPa
T_0	35 °C
$\rho\Delta s_M$	0.17 MPa.C ⁻¹
σ_U^S	120 MPa
σ_U^E	98 MPa
σ_{CL}^S	0
ε_V^T	0.06

Where: σ_L^S is the stress at the forward transformation start in tension, σ_L^E is the stress at the forward transformation end, σ_U^S is the stress at the reverse start transformation, σ_U^E is the stress at the reverse transformation end and σ_{CL}^S : is the stress at the forward transformation start in compression.

The model proposed by Auricchio is simpler in terms of number of parameters and reproducing features.

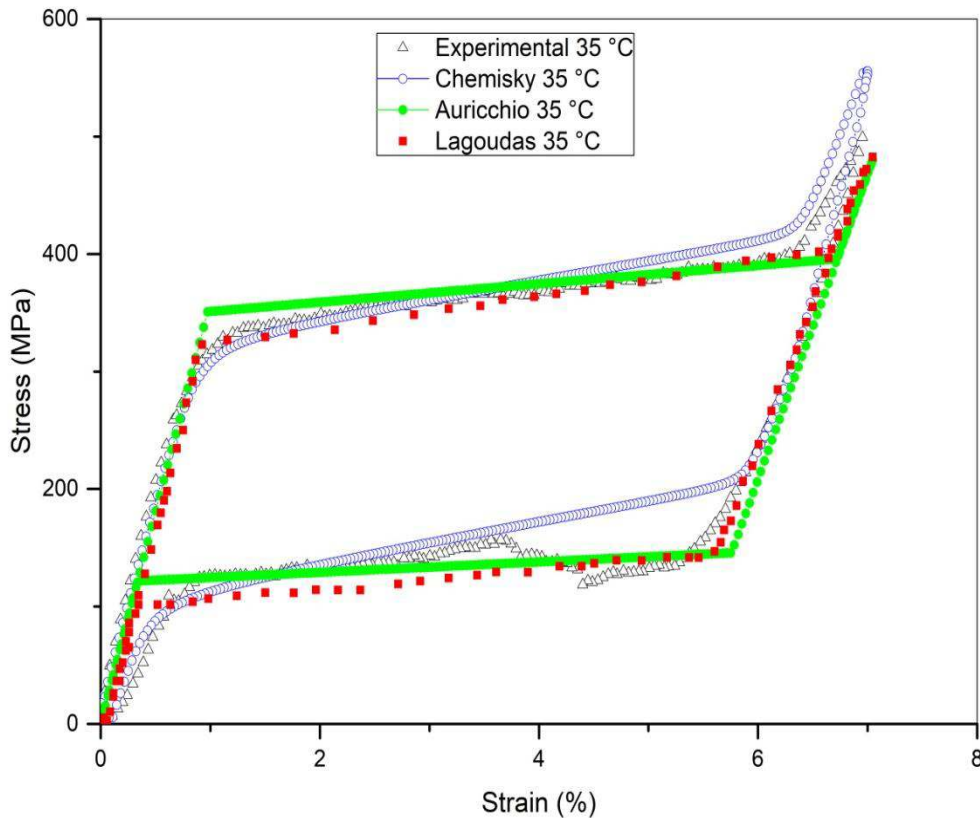


Figure 4. NiTi uniaxial tensile tests reproducing using Lagoudas and Boyd (1996), Auricchio and Petrini (2004) and Chemisky et al (2011) models and confrontation with the experimental curve at 35 °C.

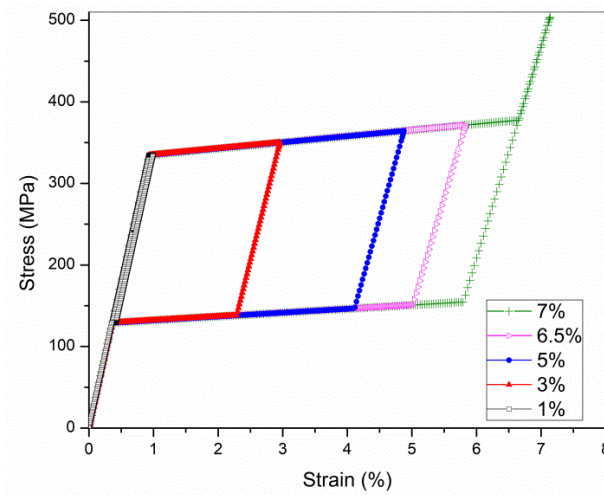
Figure 4 shows the numerical and the experimental stress–strain curves at a constant temperature of 35 °C for a 40 mm samples, cutted in an orthodontic wire. This figure shows that at a temperature above A_f , superelastic effect is ideally replicated and a complete strain recovery is obtained during the unloading end. A good accordance between experiments and simulations is obtained for the three models, as they can reproduce the main characteristics (SE) of the studied SMA. Moreover, we could observe that the strain is composed of elastic part and inelastic reversible one up to 7 %. We observe that the unloading pseudo-plateau during the reverse transformation takes place at a lower stress level about (120-160) MPa, whereas the loading pseudo-plateau is about (320-340) MPa.

In order to check that these three models are able to predict the hysteretic internal loops behavior of SMA, a tensile load was applied to a strain of 1% then followed by fully unloading and then a higher reloading up to 3%, 5%, and 6.5% or 7 % are applied followed by a fully unloading.

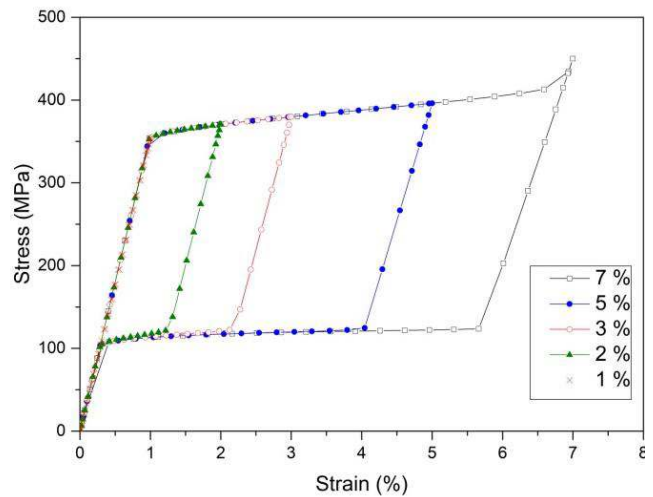
The stress-strain curves obtained from this cyclic loading test are shown in Figure 5. Some points to notice are that the model of Chemisky et al (2011) is capable to reproduce the property of internal hysteresis loops. The stress at the unloading plateau decreases with the increase of the displacement amplitude. Whereas, Lagoudas and Boyd (1996) and Auricchio and Petrini (2004) models do not allow the description of this effect observed experimentally (see Figure 2).

We could remark also that from applying strain of 1% to 3% the curves pass through the same loading points confirming the effect of return point memory (Chemisky et al 2011).

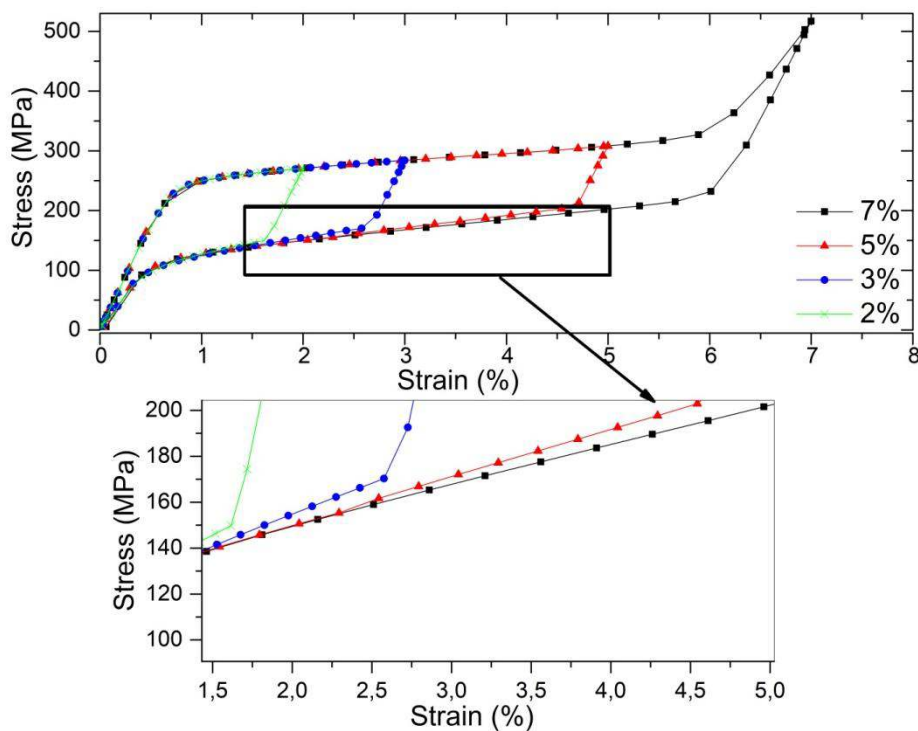
The general shape of the mechanical response by Chemisky et al (2011) model is more allied to experimental curve with a slight slope in loading and unloading plateaus. In fact, this model predicts the inner loops feature whereas this effect is less considered in Lagoudas and Boyd (1996) and Auricchio and Petrini (2004) models (Figure 5). Some applications of the SE give advantages in working on the total transformation such as the coupling sleeves (TiNi aerospace), however, an arch in the mouth can be unloaded across the pseudo-plateau of forward transformation without completing the total transformation. The unloading of the archwire depends on the distance of the irregular dentition.



(a) Lagoudas and Boyd (1996) model



(b) Auricchio and Petrini (2004) model



(c) Chemisky et al (2011) model

Figure 5. Modeled stress-strain tensile curves of NiTi orthodontic wires after four loading cycles at 1 %, 3 %, 5 % and 7% of strain with (a): Lagoudas and Boyd (1996) model, (b): Auricchio and Petrini (2004) model and (c): Chemisky et al (2011) model.

Once the wire is bent at a given strain, it is the unloading force which produces the tooth movement. The exhibited force during the reverse transformation permits to evaluate the orthodontic effect. This model is then more reliable to determinate the orthodontic load values during deflections in *mm* increments.

The next section details to the numerical simulation by finite element method of the generated loading by a SE NiTi orthodontic archwire.

3. Finite element simulation of the orthodontic loading caused by an SE NiTi archwire in a fixed appliance

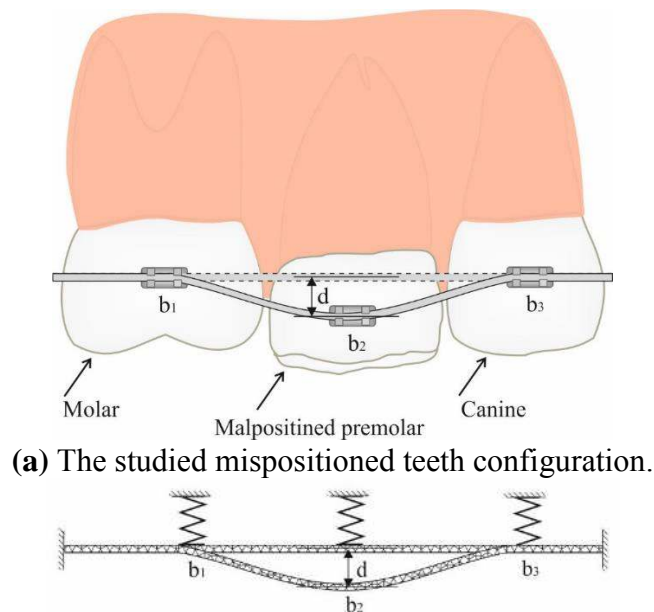
3.1. Numerical simulation of the orthodontic load in free recovery

As described below in Figure 6, the numerical configuration studied in this part is extracted from the total dental brace. We propose a SE NiTi wire to be inserted into the slot of a bracket bonded to a tooth.

The applied displacement is of a 2 mm, 4 mm and 6 mm on a $0.46 \times 0.64 \text{ mm}^2$ cross section wire with a $0.67 \times 0.67 \text{ mm}^2$ bracket slot section. The bending test simulates the wire stimulation on the teeth in the oral cavity. Deflections are chosen in order to compare our results with other studies (Wilkinson et al 2002, Parvizi and Rock 2003, Arghavani et al 2010 and Lombardo et al 2012). As aforementioned, the objective of performing this simulation is to numerically predict the orthodontic force applied by the orthodontic archwire on the bracket. This force will be subsequently able to cause the dental displacement.

A loading-unloading test is simulated at the oral temperature 35°C under displacement control. The simulation is performed using quadratic hexahedral elements (C3D20). A convergence analysis is one made to choose the optimal elements size by considering the load-displacement response as the convergence criteria. A bias mesh was added to refine the mesh.

The tooth and the metal bracket are modeled like a unique deformable body (see Figure 8). Contact elements permit the interaction between the parts. It is desirable that the wire moves into the bracket with a minimum of friction. A friction coefficient of 0.3 was taken from the literature (Noda et al 1993).

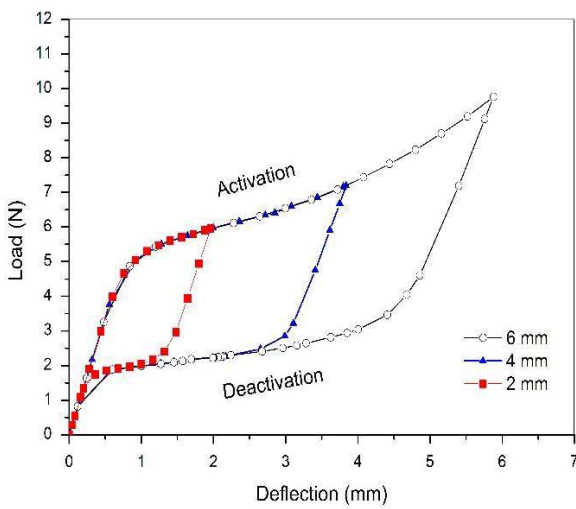


(b) Boundary conditions and load applied to the three-dimensional orthodontic wire.

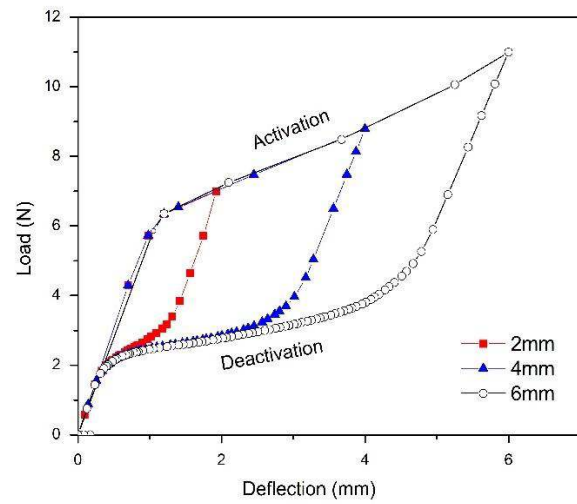
Figure 6. The studied malocclusion configuration.

Figure 6 shows the rectangular cross section $a \times b$ mm² wire and the applied boundary conditions. In order to simplify the model, we consider the smallest dental unit with a straight portion of the archwire inserted in a molar, a premolar and a canine. The **b1** and **b3** indications designate the two fixed brackets on the molar and the canine, the **b2** indicates the mis-positioned tooth that was removed of a distance **d** from its appropriate position. The material parameters of the three considered models are identified from the tensile tests and listed in Tables 3 to 5.

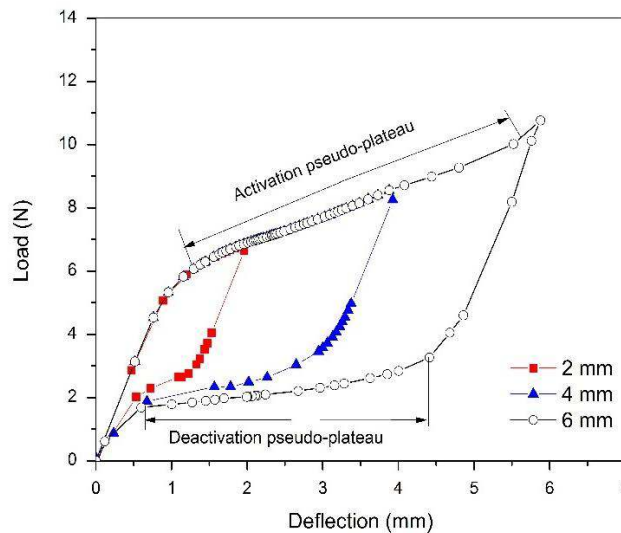
Figure 7 compares the load-deflections curves of the three considered models for different deflections at 35 °C. As it depicted, since the tested temperatures are greater than A_f ($T > A_f$), the strain is fully recovered after a total unloading which reflects the superelastic behavior.



(a) Lagoudas and Boyd (1996) model



(b) Auricchio and Petrini (2004) model

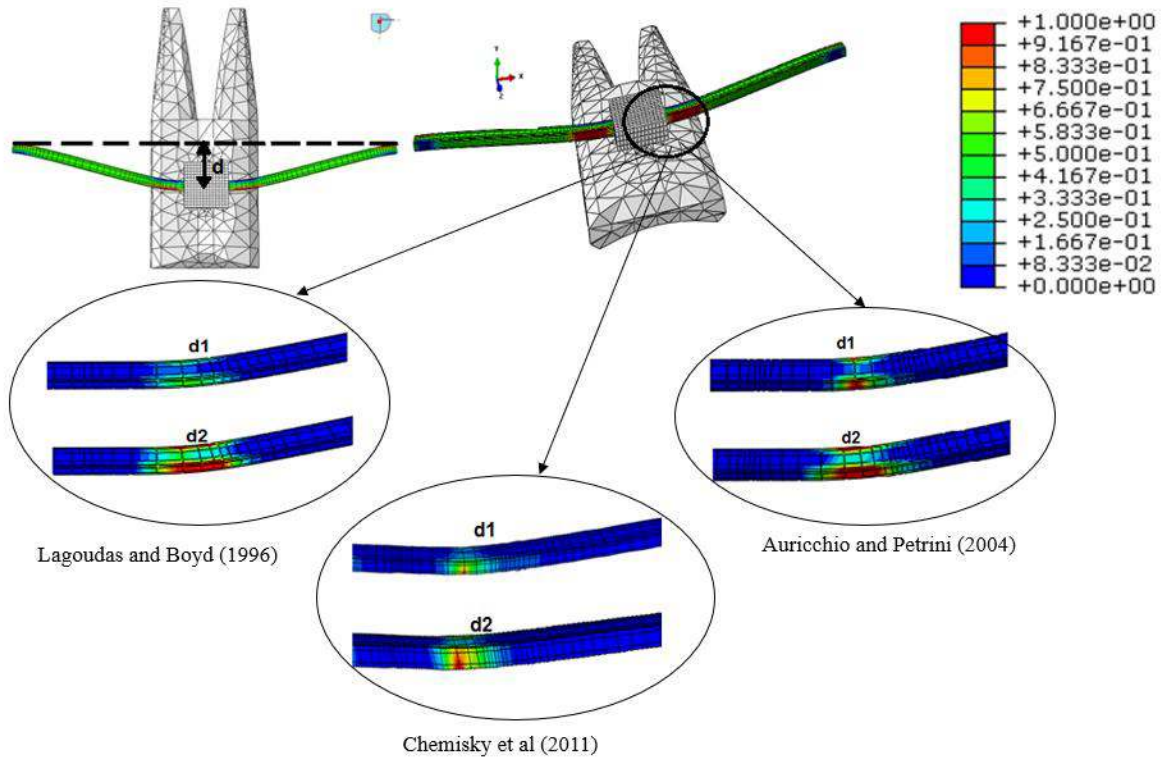


(c) Chemisky et al (2011) model

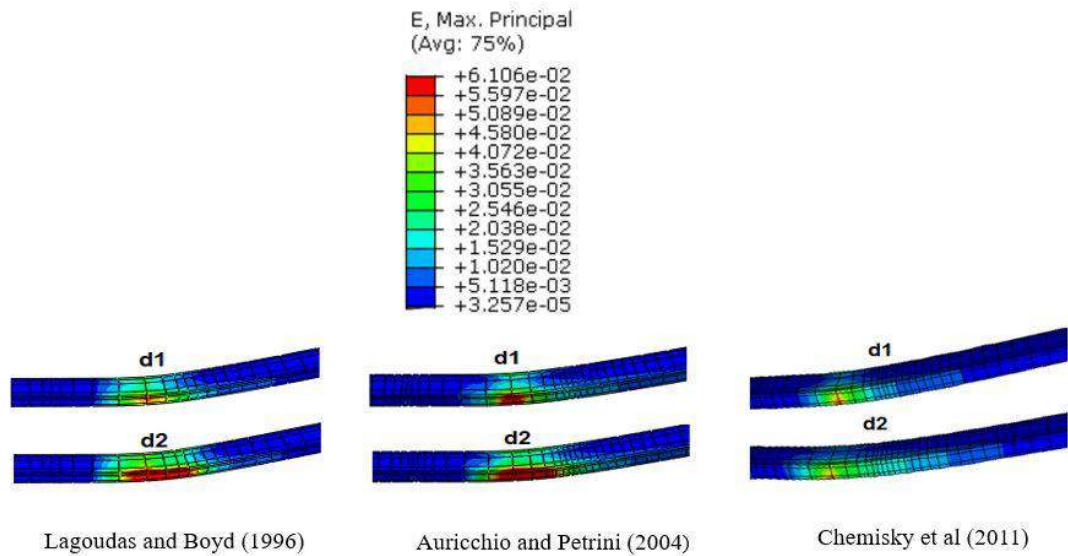
Figure 7. Modeled of orthodontic load at 35 °C in a real orthodontic malocclusion chosen case at 2mm, 4mm, and 6mm of imposed displacement (a) Lagoudas and Boyd (1996) model, (b) Auricchio and Petrini (2004) model and (c) Chemisky et al (2011) model.

In particular it is observed in Figure 7 (c) the inner loop feature description. In fact, the curves being deflected at different controlled strains have the same activation curve. Whereas, through deactivation curve, the response has showed a different unloading curves which depend on the applied deflection. The deactivation curve (Figure 7) indicates the load generated by wire to displace the tooth to its self-position. Those results imply that the archwire doesn't exert the same load level with different deflections. Thus, if the wire in each mispositioned dental configuration is working on a point of this pseudo-plateau, the treatment would be more effective to dental movement.

In consequence, the wire deflected from 2 mm to 6 mm reproducibly can generate a constant force to large misaligned teeth. Therefore, it permits to keep a same archwire for a long period of treatment. According to those considerations when orthodontists deactivate a wire to a 2 mm of deflection from its initial 4 mm or 6 mm bracket position, they obtain a load lower than the one activating the same wire to 2 mm.



(a) Martensite volumetric fraction at an imposed deflection $d_1=2$ mm and $d_2=4$ mm



(b) Strain at the end of the loading phase

Figure 8. Martensite volume fraction distribution (a) and strain distribution on the archwire (b) at the end of the loading step at 35°C simulated by Lagoudas and Boyd (1996) model, Auricchio and Petrini (2004) and Chemisky et al (2011) models.

Figure 8 (a) presents the martensitic volume fraction distribution in the superelastic wire upon 2 mm and 4 mm of loading step at 35 °C. First, we note that some regions are totally transformed to martensite indicating magnitude values around 1. These regions are located where the arc is bent and respect the boundary conditions. In the other areas, the values are near to 0 magnitudes where the material is at the austenite state. Between the 1 and 0 values are the zones where a partially transformed martensite-austenite occurs. Second, we note that the three models show different volume fraction of martensite distributions. This could be resulted by the existing differences in the three formulations (Table 1).

Figure 8 (b) shows the maximum strain distribution E_{max} of the wire during the loading step at 35 °C. The zones with high values (red zones) around the regions of contact with brackets are under tension and areas between teeth in blue are in compression which is in concordance with the martensitic fraction distribution.

Figure 9 compares the load generated by a 0.64 x 0.46 mm² cross section SMA wire recorded by the three considered models at 2 mm, 4 mm and 6 mm of deflection. Finite element simulations with the three models lead to a range load average values at 2 mm, 4 mm and 6 mm of deflection from 2.7 N to 3.7 N which is within the range of the normalized orthodontic load values [0.15 N-5 N] (Rock and Wilson 1988). The numerical force levels obtained by Lagoudas and Auricchio models are quasi constant for the imposed deflections. Whereas, the force amplitude delivered with Chemisky model simulations is decreased at 6mm of deflection.

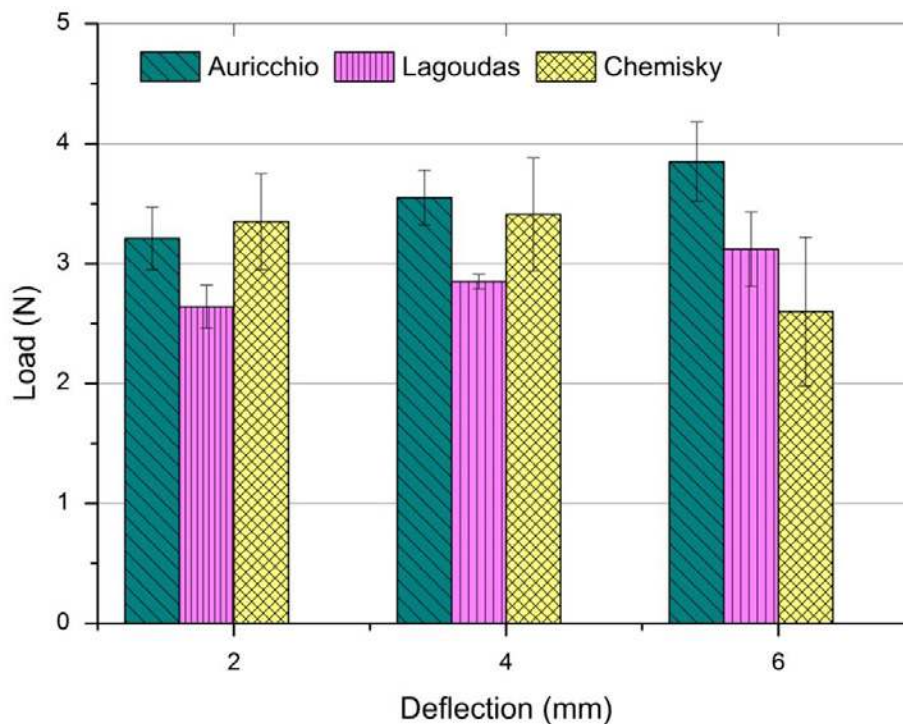


Figure 9. Graph of the orthodontic load values at 2 mm, 4 mm and 6 mm for Chemisky et al (2011), Lagoudas and Boyd (1996) and Auricchio and Petrini (2004) models at 35°C.

The load-deflection curves displayed in Figure 10 with a 2 mm of deflection at 35 °C show an approximate agreement in the response between the three considered models. This agreement is in decrease as the deflection increase (Figure 9, Figure 7).

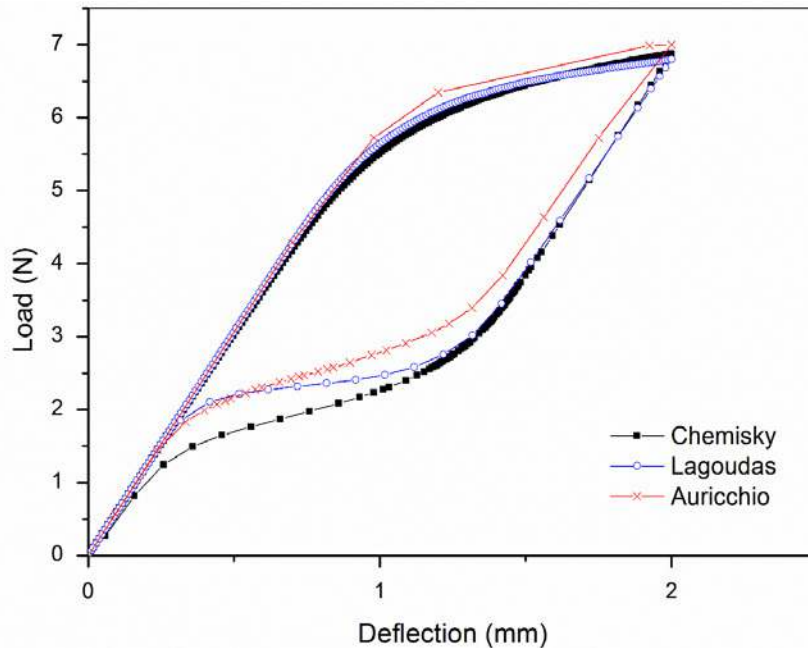


Figure 10. Load-deflection curves of 2 mm-imposed deflection for Chemisky et al (2011), Lagoudas and Boyd (1996) and Auricchio and Petrini (2004) models at 35 °C.

We move on at the next section to investigate the orthodontic level in a strain recovery. We will simulate the effect of the alveolar bone as an obstacle to the dental displacement.

3.2. Numerical simulation of the orthodontic load in a strain recovery

A numerical study was carried out to predict the orthodontic load exerted by the wire when we modulate the bone as an important component in the dental brace.

The wire is subjected to this thermomechanical loading:

- i) Activation: applying a displacement along Z axis on the contact wire between wire and bracket; while we define a constant temperature 35 °C;
- ii) Deactivation: inactivation of the imposed displacement, the surfaces extremities were clamped ($U_x=U_y=U_z=0$);

In a second step of tests, the model was modified in order to take into consideration the insertion of the tooth into the bone. The alveolar bone is considered as an obstacle to the tooth to return to its appropriate position, modulated by n springs of stiffness K_i , $i=1 \dots n$ with n is the number of nodes in contact with the bone (see Figure 6). Numerical simulations on Abaqus software permit the determination of approached values of the bone stiffness with values in [0.016 N/mm-2 N/mm]. We varied the bone stiffness values in order to verify their effect on the load level.

Figure 11 shows that the tooth displacement is blocked as closer to the initial position as the bone stiffness value decreased. Those simulations are reproduced by Auricchio and Lagoudas models to gain the cost of simulation using the configuration shown at Figure 8 as we will determinate mainly the effect of bone stiffness on the orthodontic load.

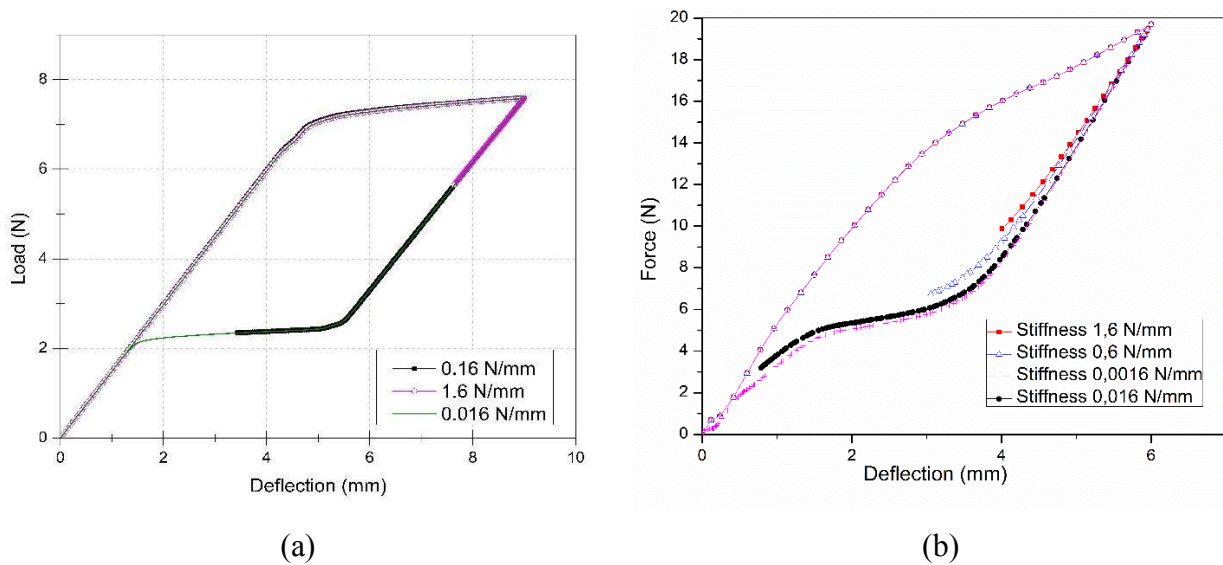
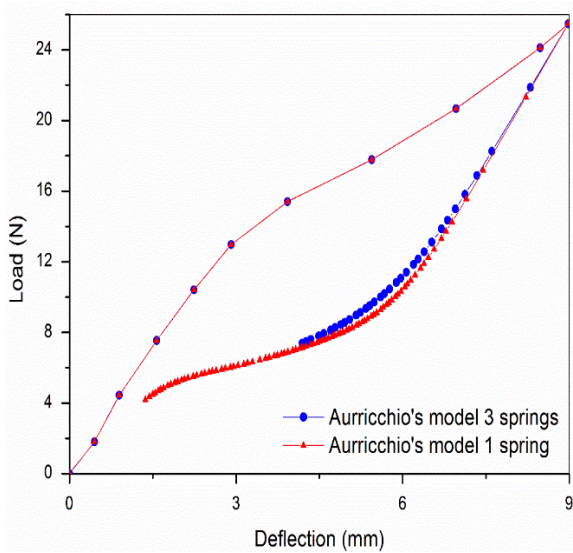


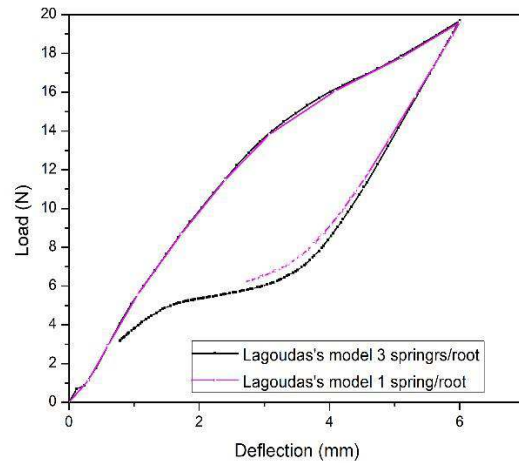
Figure 11. The effect of the alveolar bone stiffness on the load-deflection response curves with (a) the simplified configuration and (b) the tooth/bracket assembled.

The variation of the number of springs affected also the displacement of the dental movement as shown in Figure 12. Those numerical results demonstrate that the wire estimated force shows significant difference by different type of tooth. In consequence, the practitioner should mind to the age of the patient and the tooth nature in clinics.

Figure 11 and Figure 12 summarize the effect of the alveolar bone stiffness to resist to a dental displacement. The tooth movement is clamped as the stiffness increases. For instance, if the stiffness valued 1.6 N/mm, the wire didn't reach the deactivation plateau, which means that the wire is nonfunctional for the considered treatment situation. Hence an increase in the wire section could enhance the dental correction.



(a)



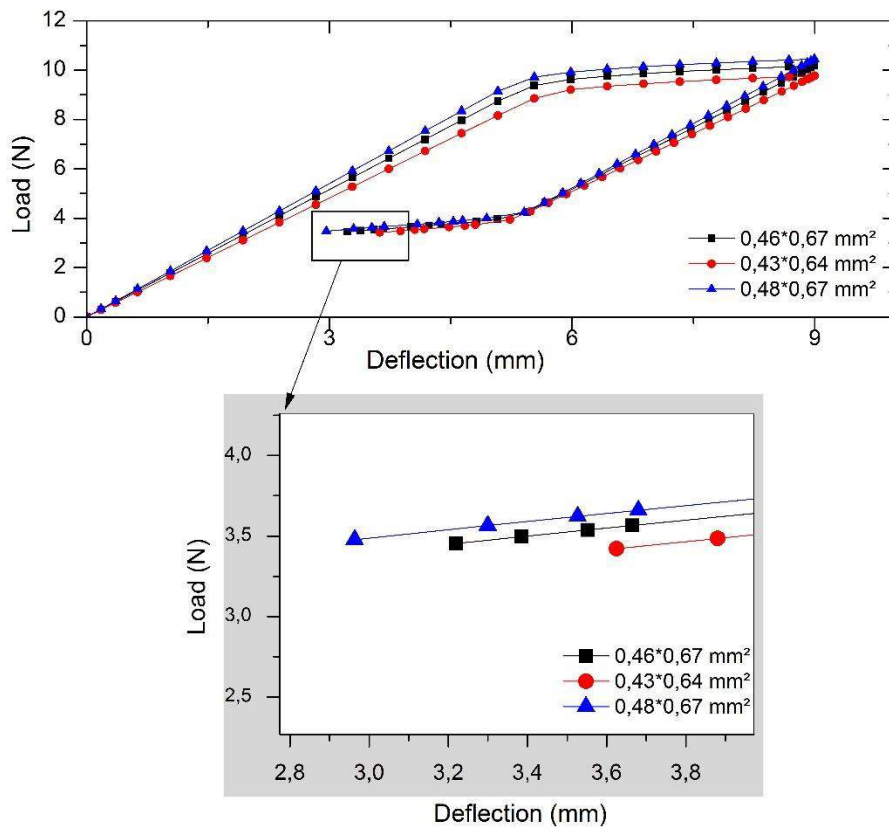
(b)

Figure 12. Load-deflection curves response to 0.16 N/mm alveolar bone stiffness at 35 °C with the variation of the number of contact with bone using (a) Aurrichio model and (b) Lagoudas model

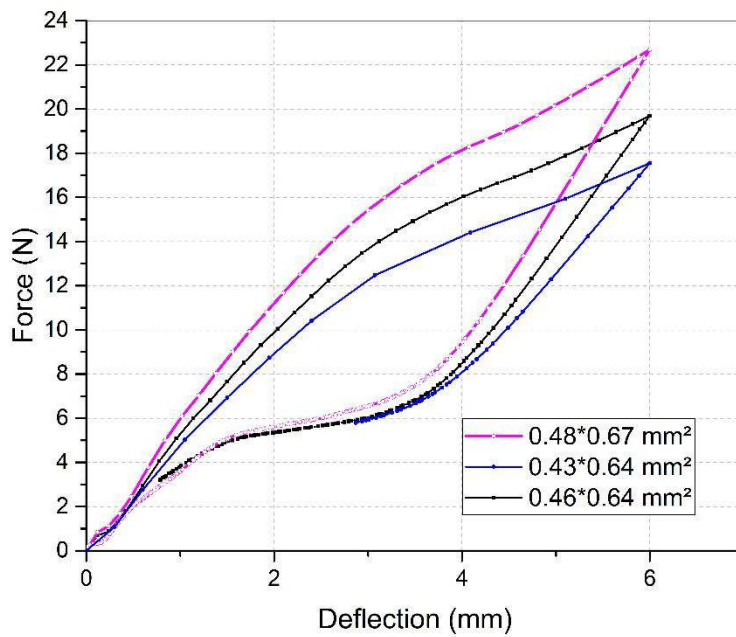
Figure 13 shows that the increase in the cross section of the wire induces the reverse martensitic transformation despite the load increase. In consequence, a higher cross section wire induces more reverse transformation and consequently increases the dental displacement range. This is explained by the higher formed martensite volume fraction which leads to the elevation of the stored energy and hence induces the reverse transformation (Garrec et al 2005). Clinically, the practitioner should choose wisely the section of the used orthodontic wire to ensure an adequate treatment.

Figure 14 displays the load-deflection curve recorded at 6 mm of displacement; the point *A* labels the activation of the wire to 2 mm with almost loading level of 9 N. In point *B*, the wire is loaded to 6 mm as shows the displacement *U* distribution, the loading level is about 16 N. When the archwire is unloaded, the bone with 0.16 N/mm of stiffness represents an obstacle and the deflection is blocked at 3.3 mm from the proper distance in point *C* and therefore the wire could not recover its initial position. The SMA displays advantages if the archwire working area is on the plateau and not in the austenite linear phase.

Figure 14 shows as well that patients who expose very irregular mis-positioned dental configuration offer the advantage to have a ‘soft’ treatment, below this deflection the SMA will behave as a conventional elastic behavior.



(a) Simple configuration curves (Figure 6 (b))



(b) assembled tooth/arc configuration curves (Figure 8)

Figure 13. The effect of the rectangular cross section wire on the orthodontic load (a) the simple configuration (b) the assembled tooth/arc configuration

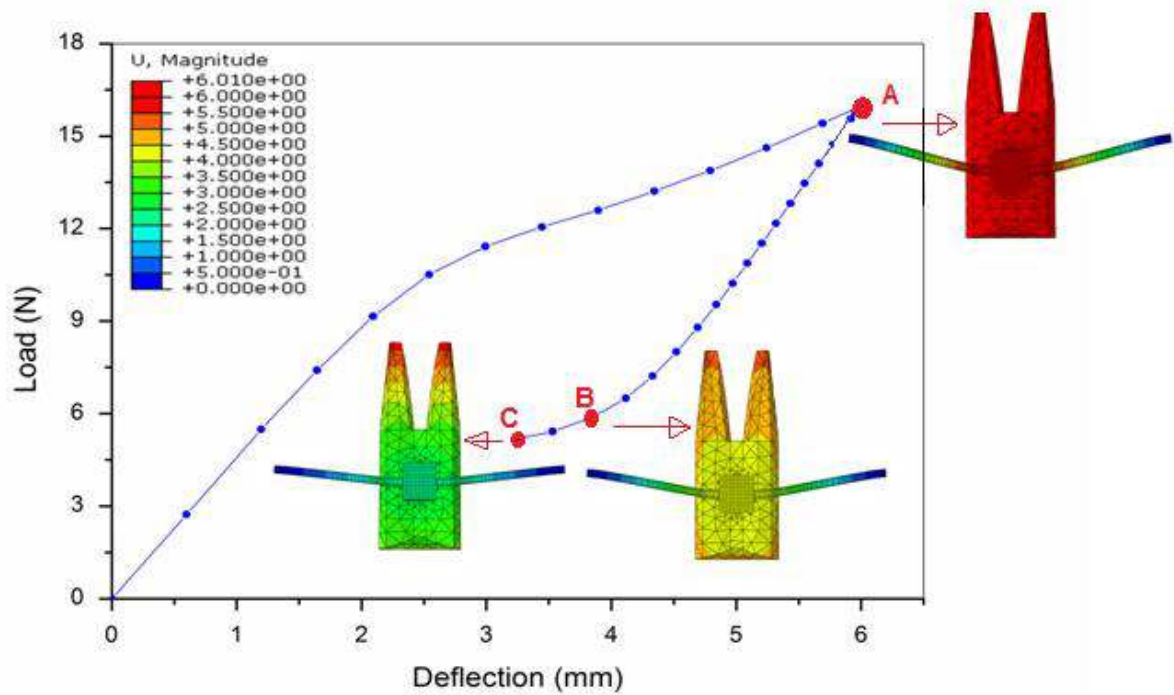


Figure 14. Load-deflection response to 6 mm of deflection control and the displacement recovered by tooth at different steps.

In the next section, we will determine the effect of the temperature alterations on the orthodontic load.

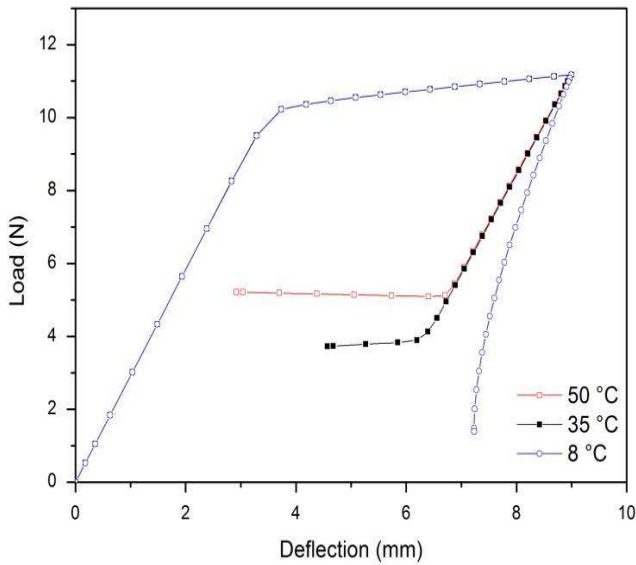
3.3. Numerical simulation of orthodontic load and final tooth displacement: temperature effect

The human oral temperature approximates 35 °C but many factors usually could affect the oral temperature including the ingestion of cold or hot substances, external temperature and humidity, smoking and whether the mouth is open or closed (Moore et al 1993).

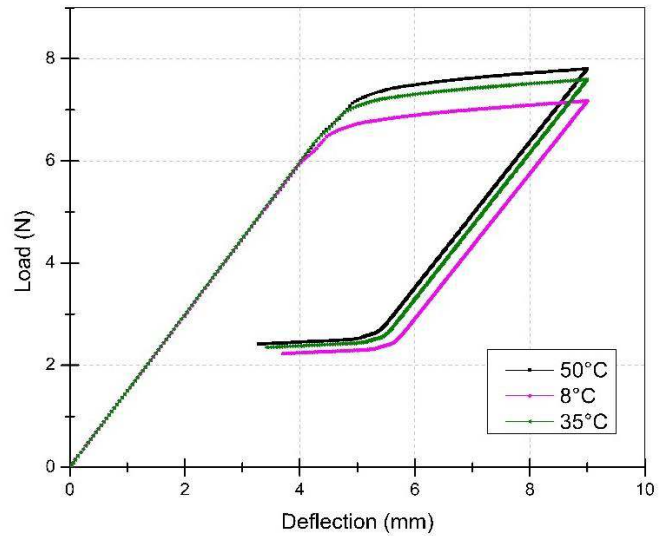
The load-deflection behavior of a NiTi SE archwire has been examined in the bending configuration over the temperature range [8 °C-50 °C]. This chosen range is correlated with the investigation of Moore et al (1993) that recorded 24 hours intra-oral temperature. In this investigation we kept constant tooth stiffness at 0.16 N/mm. The selected temperatures to carry out the study were 8 °C, 25 °C, 35 °C, and 50 °C.

Figure 15(a), 15(b) and 15(c) represent respectively the load-deflection responses to 9 mm of deflection (figure 16, Burstone and Koenig 1974). The models exhibit similar response against the temperature variations: the stress at loading and unloading plateaus increase as the temperature increases. The wire is loaded with 9 mm of deflection at the oral temperature, during the unloading step the temperature is increased to 50 °C or decreased to 8 °C. Obtained numerical response leads to the following features: i) the orthodontic force delivered during the unloading of archwire increased

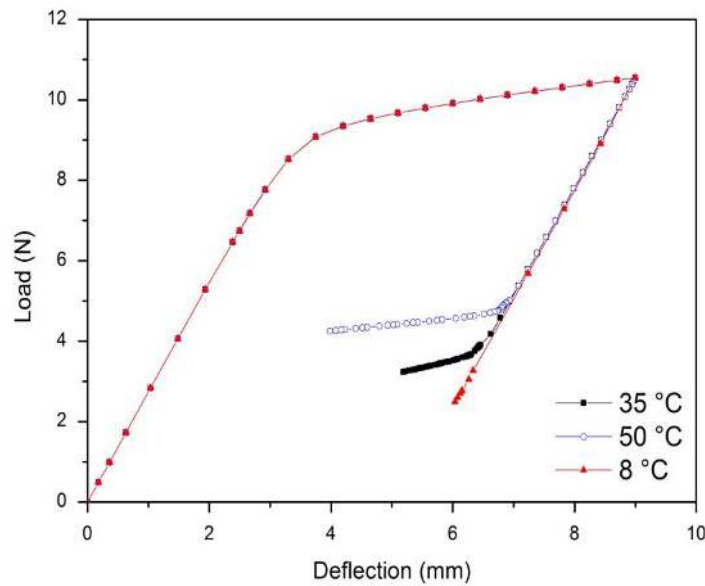
with the temperature increase, ii) the slope of the unloading plateau decreased with the temperature increase, iii) below a critical temperature, the wire showed a residual strain without an unloading plateau and iv) the load and the displacement covered by tooth increase as the temperature increases.



(a) Lagoudas and Boyd (1996)



(b) Auricchio and Petrini (2004)



(c) Chemisky et al (2011)

Figure 15. Effect of temperature on a wire deflected to 9 mm of displacement and resisted to a 0.16 N/mm of tooth stiffness by the three considered models

Figure 16 shows the load-deflection response of the archwire loaded at 35 °C and unloaded at 8 °C, 35 °C and 50 °C by Auricchio's model. The wire is bounded to brackets attached to teeth, with a 0.16 N/mm stiffness (Figure 8). In comparison with the load-deflection response of the wire in the simplified configuration described in Figure 6, the plateau region extent, gradient of tooth displacement to the proper position and the load values varied. Therefore, the load depends on the

orthodontic configuration, Wilkinson et al (2002) shows that the load depends on the design of test configuration. Regardless of the bone stiffness, the force value increases with temperature increasing. These phenomenon are explained referring to clausius–clapeyron diagramm which gives a linear relationship between T and σ . These results confirm those reported by Ijima et al (2002).

Figure 15 (b) reproduces the wire as a beam resited to springs reactions and the figure 16 considers the wire assembled in a configuration closely ressembled to a clinical configuration. This result implies that considering the wire as a beam in the numerical study a little bit-underestimates the orthodontic loads.

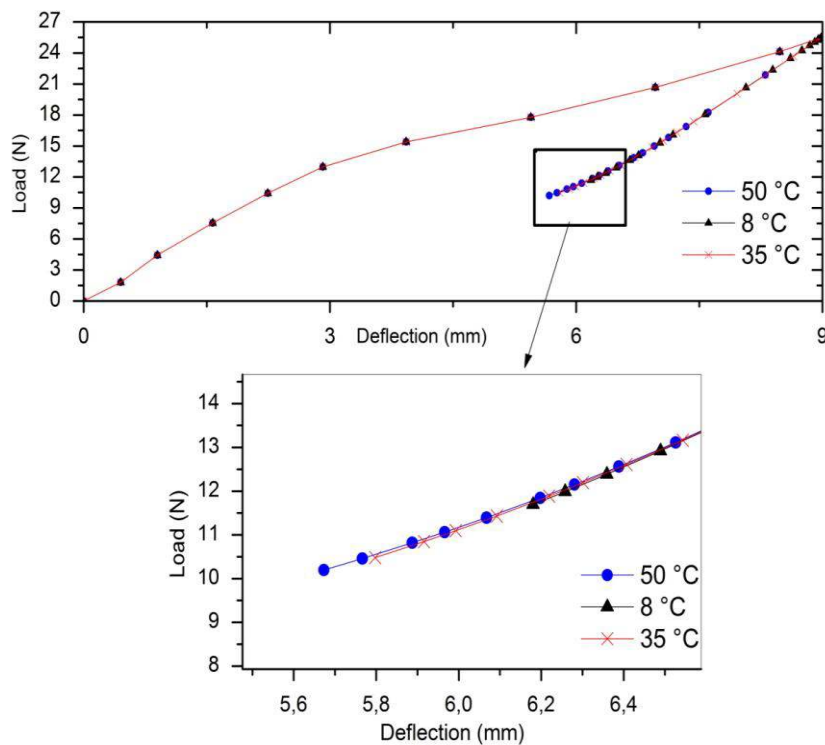


Figure 16. Effect of temperature on the deactivation plateau the load-deflection curve of the NiTi SE wire deflected at 9 mm (Auricchio and Petrini model 2004).

Table 6 summarizes the orthodontic forces which are predicted with a 3 mm and 6 mm applied deflections at 8 °C, 35 °C, and 50 °C. These values demonstrated that the increase in temperature increases the orthodontic generated load and induced more martensitic transformation. Otherwise, Table 7 presents the distance covered by the tooth generated by the same imposed deflections with a 0.16 N/mm alveolar bone stiffness.

Compared to Ben Naceur et al (2014), the 0.64 x 0.46 mm² wire delivers for 2 mm deflection control at 35 °C we present approximately close load values at activation and deactivation (Figure 7), it may be due to the difference in model design.

Table 6. Load values (N) at 6 mm and 3 mm deactivation points of an archwire being activated to 9 mm, the bone stiffness is 0.16 N/mm at 8 °C, 35 °C, 50 °C.

	Lagoudas and Boyd (1996) model		Auricchio et Petrini (2004)		Chemisky et al (2011)	
	3 mm	6 mm	3 mm	6 mm	3 mm	6 mm
35 °C	3.95	3.90	7.32	5.24	-	3.28
50 °C	5.14	5.24-	7.30	5.12	4.94	4.74
8 °C	-	-	7.92	4.90	2.72	-

Referring to Figure 15 we could extract more information about the influence of the temperature on the orthodontic load and the distance traveled by the tooth to recover its appropriate position.

Table 7. Distance covered by the tooth when it is unloaded of 9 mm deflection at different 50 °C, 35 °C and 8 °C temperatures. The alveolar bone stiffness is 0.16 N/mm.

Model	Lagoudas and Boyed (1996)			Auricchio and Petrini (2004)			Chemisky et al (2011)		
	50°C	35°C	8°C	50°C	35°C	8°C	50°C	35°C	8°C
Displacement of tooth (mm)	6.35	4.65	1.83	7.15	6.05	5.87	5.27	4.77	2.95

According to Khier et al (1991), the wire is in austenite phase, the deflection causes the martensitic transformation and generates the stress induced martensite (SIM), the SIM is formed in the stressed areas in the wire (Figure 8 (a)), where is engaged to brackets bounded to mis-positioned tooth. When we keep a constant temperature, the martensite permits to wire to be more pliable. Therefore, forces will decrease in needed zones. After tooth movement to its appropriate position, the wire self-restores by the austenitic phase. When the temperature increases above the oral temperature, the SE SMA exhibits higher load in deactivation to transform to austenite. The temperature at which an appeared permanent strain could correspond to a stable SIM and the transformation is then impossible (Ferreira et al 2012, Tonner et al 1994).

These elevations or decreases in temperature lead to a variable range of forces with consequent painful or relaxation sensations that could affect the effectiveness of treatment. According to the previous numerical simulation results, we could affirm the interest role of the numerical simulations in the orthodontic load estimations. The considered models were lead to different results depending on the considered formulation, because they neglect some physical aspects of the superelastic behavior (Cisse et al 2016).

The numerical simulation of an orthodontic archwire in physiological conditions is intricate because not only the tooth/bracket configurations and the reaction of the bone stiffness are complicated to represent (Shiva and Hosseini 2012), but also the consequence of the temperature alterations at mouth due to different taken food or drinks should be considered.

5. Conclusions

In this paper, we present a comparative numerical simulation of three different SMA constitutive models in order to simulate by finite element method mainly a $0.64 \times 0.46 \text{ mm}^2$ cross section wire response. The three considered models had successfully reproduced the SE behavior of the NiTi archwire. The loading curve represents the force that is required to insert the wire in the bracket bounded to a misaligned tooth. This force is usually measured at the last deflection of the loading curve. Whereas, this unloading curve represents the force delivered to correct this misalignment. Usually this deactivation load is measured in several deflection points during the therapy. We notice that the load-deflection curves show different performances depending on the constitutive model. This difference may be due to the considered features and modeled approaches.

In addition, the SE numerical simulations highlight the sensitivity of the mechanical response to the temperature. Actually, the temperature change induces the martensitic transformation which modifies the placed force on tooth. Hence, the wire in a mouth is influenced by the temperature alterations. Moreover, the numerical results show that under a critical temperature the SE behavior does not present any deactivation plateau.

Moreover, the numerical investigations show that the bone stiffness is an important parameter in the measure of the orthodontic load generated by the wire to correct a misaligned tooth. Under certain conditions, this stiffness can be an obstacle to the tooth proper position displacement.

Additionally, the rectangular archwire with a larger cross section displays an advantage to induce the reverse transformation and therefore to imply the tooth movement which is controversial to Khier et al (1991) results. Indeed, a high cross section wire risks to generate a higher level of the orthodontic force which could be not permissible to the biological tissue. However, a low applied force level could be insufficient to cause the tooth movement. The obtained numerical simulations show that the increase in deflection, which corresponds to the degree of the tooth irregularity, leads to a reduction of the orthodontic load in correction phase.

We obtained through the analyzed numerical simulations that the force level is within the acceptable values to be exerted by an archwire but isn't in the desired force range $[0.05 \text{ N}-1 \text{ N}]$ (Rudolf et al 2013). This cross section is therefore oversized. The numerical simulations show that the force exerted continuously and at constant level could influence the bone remodeling and exhibits more attention to restrict the load at a desired limit. On the basis of those simulations, we could recommend the orthodontists to advice their patients to decrease the temperature in order to decrease the force level. This can be performed by drinking fresh drinks when a certain discomfort is felt.

Actually, these numerical simulations are to be used as a decision-help tool in favor of the orthodontist to define the optimal archwire cross section dimensions depending on the needed correction and the operative temperature range.

In Perspectives, an experimental study would be useful to validate these findings. Due to the relatively large intra- and inter- oral conditions, other tests on different sample sizes and compositions are required within different test temperatures.

References

- Aghili H, Yassael S, Ahmadabadi M N and Joshan N 2015 Load deflection characteristics of Nickel Titanium initial Archwires *J. Dent.* 12 695-705
- Aghili H, Yassael S and Eslami F 2017 Evaluation of the effect of three mouthwashes on the mechanical properties and surfaces morphology of several orthodontic wires: an in vitro study *Dent. Reach. J.* 14 252-259
- Andreasen G F and Hilleman T B 1971 An evaluation of 5.5 cobalt substituted nitinol wire for use in orthodontics *Am. J. Dent. Assoc.* 82 1373-1375
- Arghavani J, Auricchio F, Naghadabi R, Reali A and Sohrabpour S 2010 A 3-D phenomenological constitutive model for shape memory SMAs under multiaxial loadings *Int. J. Plast.* 26 976-991
- Auricchio F and Petrini L 2004 A three-dimensional model describing stress-temperature induced solid phase transformations: solution algorithm and boundary value problems *Int. J. Numer. Meth. Engng.* 61 807-836
- Ben Naceur I, Charfi A, Bouraoui T and Eleuch K 2014 Finite element modeling of superelastic nickel-titanium orthodontic wire *J. Biomech.* 47 3630-3638
- Bourauel C, Drescher D and Thier M 1999 An experiment apparatus for the simulation of three dimensional movements in orthodontics *J. Biom. Eng.* 14 371-378
- Bouvet C, Calloch S and LExcellent C 2004 A phenomenological model for pseudoelasticity of shape memory alloys under multiaxial proportional and nonproportional loadings. *European Journal of Mechanics A/Solids* 23 37-61
- Burstone C J and Koenig H A 1974 Force systems from an ideal arch *Am. J. Orthod.* 65 270-291
- Cisse Ch, Zaki W and Ben Zineb T 2016 A review of constitutive models and modeling techniques for shape memory SMA *Inter. J. Plast.* 76 244-284
- Chemisky Y, Duval A, Patoor E and Ben Zineb T 2011 Constitutive model for shape memory SMAs including phase transformation, martensitic reorientation and twins accommodation *Mech. Mater.* 68 361-376
- Dolce M and Cardone D 2001 Mechanical behavior of shape memory alloys for seismic applications 2. Austenite NiTi wires subjected to tension. *Int. J. of Mechanical Sciences* 43 2657-2677
- Ferreira M A, Luersen M A and Borgos P C 2012 Nickel-titanium SMAs: A systematic review *Dental Press. J. Orthod.* 17 71-82
- Gamaoun F, Ltaeif M, Bouraoui T and Ben Zineb T 2011 Effect of hydrogen on the tensile strength of aged Ni-Ti superelastic alloy *J. Intell. Mater. Syst. Struct.* 22 2053-2059
- Garrec P, Tavernier B and Jordan L 2005 Evolution of flexural rigidity according to the cross-sectional dimension of a superelastic nickel titanium orthodontic wires *Eur. J. Orthod.* 27 402-407
- Gillet Y, Patoor E and Berveiller M 1998 Calculation of pseudoelastic elements using a non-symmetrical thermomechanical transformation criterion and associated rules *J. of Intelligent Mater. Syst. and Struct.* 9(5) 366-378

- Ijima M, Ohno H, Kawashima I, Endo K and Mizoguchi I 2002 Mechanical behavior at different temperatures and stresses for superelastic nickel-titanium orthodontic wires having different transformation temperatures *dent. Mat.* 18 88-93.
- Khier S E, Brantley W A and Fournelle R A 1991 Bending properties of superelastic and non superelastic nickel-titanium orthodontic wires *Am. J. Orthod. Dentofac. Orthop.* 99 310-318
- Lachiguer A, Bouby C, Gamaoun F, Bouraoui T and Ben Zineb T 2016 Modeling of hydrogen effect on the superelastic behavior of NiTi shape memory SMA wires *Smart. Mater. Struct.* 25 115047 (11pp)
- Lagoudas D C and Boyd J G A 1996 thermodynamical constitutive model for shape memory materials 1996 *Int. J. Plast.* 12 805-842
- Lombardo L, Marafioti M, Stefanoni F, Mollica F and Siciliani G 2012 Load-deflection characteristics and force level of nickel titanium initial archwires *Ang. Orthod.* 82 507-521
- Miura F, Mogi M, Ohura Y and Hamanka H 1986 The superelastic property of the Japanese NiTi SMA wire for use in orthodontics *Am. J. Dentfac. Orthop.* 90 1-10
- Moore R J, Watts T F J, Hood A A J and David J B 1999 Intra-oral temperature variation over 24 hours *Eu. J. Orthod.* 21 249-261
- Muller I 1989 On the size of the hysteresis in pseudoelasticity *Cont. Mech. Thermod.* 1 125-142
- Noda T, Okamoto Y and Hamanaka H 1993 Frictional property of orthodontic wires-evaluation by static frictional coefficients *J. Jpn. Orthod. Soc.* 52 154-160
- Parvizini F and Rock W P 2003 The load/deflection characteristics of medical-grade Nitinol wire *Eur. J. Ortho.* 25 417-421
- Peultier B, Ben Zineb T and Patoor E 2006 Macroscopic constitutive law of shape memory alloy thermomechanical behavior. Application to structure computation by FEM *Mec. of Mater.* 38 510-524
- Rock W P and Wilson H P 1988 Forces exerted by orthodontic aligning arch wires *Brit. J. Ortho.* 15 255-259
- Rudolf R T and Fercec J J 2013 Forces measurements on teeth using fixed orthodontic systems *Vobnotechnicki Glasnik/military technical courier* 2 105-122
- Schneider J, Geiger M and Sandar F G 2002 Numerical experiments on long-time orthodontic tooth movement *Am. J. Orthdo. Dentfac. Orthop.* 121 257-265
- Segner D and Ibe D 1995 Properties of superelastic wires and their relevance to orthodontic treatment *Eur. J. Orthodo.* 17 395-402
- Shiva A and Hosseini N 2012 Load-deflection and surface properties of coated and conventional superelastic orthodontic archwires in conventional and metal-insert ceramic brackets *Dent. Res. J.* 9 133-138
- Souza A C, Mamiya E N and Zouain N 1998 Three-dimensional model for solids undergoing stress-induced phase transformations *Eur. J. of Mecha.* 17 789-80
- Tanne K, Sakuda M and Burstone C J 1987 Three-finite element analysis for stress in the periodontal tissue by orthodontic forces *Am. Ortho. Dentofacial Orthop.* 92 499-505
- Tonner R I M and Waters N E 1994 The characteristics of superelastic NiTi wires in three-point bending. Part I: The effect of temperature *Eu. J. Orthod.* 16 409-419
- Their M, Treppmann D, Drescher D and Boureaul C 2004 Transformation characteristics and related deformation behavior in orthodontic NiTi wire *J. Mater. Science: Mater. In medicine* 3 229-233
- Wilkinson P D, James S D, Hood A A and Herbison G P 2002 Load-deflection characteristics of superelastic nickel-titanium orthodontic wires *Am. J. Orthod. dentofac. Orhtop.* 121 483-495